MATERIALS CHEMISTRY
FRONTIERS

RESEARCH ARTICLE

View Article Online
View Journal | View Issue

Cite this: *Mater. Chem. Front.*, 2018, **2**, 573

Modulation of luminescence chromic behaviors and environment-responsive intensity changes by substituents in bis-*o*-carborane-substituted conjugated molecules†

Hiroki Mori, Kenta Nishino, Keisuke Wada, Yasuhiro Morisaki, ‡ Kazuo Tanaka * and Yoshiki Chujo*

Received 23rd October 2017,
Accepted 10th January 2018

DOI: 10.1039/c7qm00486a

rsc.li/frontiers-materials

Two types of multi-functional emissive bis-*o*-carborane-substituted 1,4-bis(phenylethynyl)benzene molecules were synthesized, and their optical properties were investigated in detail. The pristine *o*-carborane-substituted molecule **CBH** simultaneously exhibited dual emission from the locally excited (LE) and twisted intramolecular charge transfer (TICT) states in solution. Originating from changes in the intensity ratios between both emission bands, clear solvatochromic and thermochromic behaviors were observed. Surprisingly, TICT emission was observed even in the solid state. Aggregation- and crystallization-induced emission enhancement (AIEE and CIEE, respectively) were also presented by **CBH**. These solid-state emission enhancements could be derived from the suppression of aggregation-caused quenching (ACQ) by the bulky cage structure and the spherical shape of *o*-carborane. Next, we also synthesized the methyl-substituted derivative (**CBMe**) and found environment-resistant highly-efficient emission in both the solution and solid states. Finally, **CBMe** presented mechanochromic luminescence in the solid state. The substituent effects on the optical properties are discussed.

Introduction

Incorporation of optically-functional "element-blocks", which are defined as a minimum functional unit containing hetero-atoms,[1,2] is a promising strategy not only for obtaining bright luminescent materials but also for showing stimuli-responsive characteristics. For example, a series of luminescent conjugated molecules and polymers has recently been developed based on luminescent boron "element-blocks".[3–5] By introducing aggregation-induced emission (AIE)-active "element-blocks"[6–8] into the conjugated main-chain, solid-state luminescence[9–13] and AIE properties[14,15] were realized in the "element-block polymers". Furthermore, by employing stimuli-responsive luminescent "element-blocks", chemical sensors and environment-sensitive luminescent chromism were also accomplished.[16–23] Therefore, discovery and exploration of unique characteristics from "element-blocks" is a topic with high relevance, especially in material science as well as in fundamental photochemistry.

From this stand point, *o*-carborane,[24–29] which is a cluster compound containing two carbon and ten boron atoms, is a potential "element-block"[30–32] for constructing a conjugated system because of its unique solid-state luminescence properties.[33–51] Moreover, it is known that the *o*-carborane units work as a strong electron acceptor when connected at the carbon.[52,53] Therefore, by combination with electron-donating aryl units, intense emission from the intramolecular charge transfer (ICT) state was often obtained.[52] In particular, it has been revealed that *o*-carborane can play a significant role in presenting solid-state emission in various systems by suppressing ACQ.[33–51] It was proposed that the steric structure of *o*-carborane should play a critical role in avoiding ACQ by disturbing intermolecular interactions with the chromophore unit. Owing to this advantage of the *o*-carborane unit, this ICT emission can often be detected from *o*-carborane derivatives with high emission efficiencies even in the solid state where emission properties were often spoiled *via* the ACQ process.[54–58] Furthermore, it was suggested from theoretical investigation that the electronic state of the *o*-carborane unit should vary by its rotation.[59] Especially, the electron-accepting ability of *o*-carborane critically depends on the angle between the C–C bond in the *o*-carborane unit and the aryl substituent.[52]

Department of Polymer Chemistry, Graduate School of Engineering, Kyoto University, Katsura, Nishikyo-ku, Kyoto 615-8510, Japan.
E-mail: tanaka@poly.synchem.kyoto-u.ac.jp, chujo@poly.synchem.kyoto-u.ac.jp

† Electronic supplementary information (ESI) available. CCDC 1581419. For ESI and crystallographic data in CIF or other electronic format see DOI: 10.1039/c7qm00486a

‡ Present address: Department of Applied Chemistry for Environment, School of Science and Technology, Kwansei Gakuin University, 2-1 Gakuen, Sanda, Hyogo 669-1337, Japan.

Based on this fact, luminescent chromism has been accomplished with π-conjugated aryl-substituted *o*-carborane structures.[60,61] Thus, the construction and evaluation of new conjugation systems connected with *o*-carborane are of great significance to discover unique photochemical phenomena as well as to develop advanced optical materials.

Herein, we present the syntheses and optical properties of bis-*o*-carborane-substituted 1,4-bis(phenylethynyl)benzene having multi-functional emissive properties. Two types of *o*-carborane derivatives with or without the methyl substituent at the adjacent carbon to the aryl moiety were prepared for evaluating the influence of molecular motion on electronic structures. From optical measurements in the solution and solid states, it was found that drastic changes can be induced by the substituents. In the absence of the substituents, dual emission from the LE and TICT states in the solution state, AIEE, CIEE and solvato- and thermochromism were observed. In contrast, the *o*-carborane derivative having methyl substituents showed constant intense emission in both the solution and solid states and mechanochromic luminescence behavior. These various useful luminescence properties can be explained by the degree of molecular motion and the structures being controlled by the substituent effect.

Results and discussion

According to Scheme 1, bis-*o*-carborane and methylated *o*-carborane-substituted 1,4-bis(phenylethynyl)benzene **CBH** and **CBMe** were synthesized, respectively. It was presumed that the molecular rotation at the *o*-carborane units would be disturbed by the methyl substituent at the adjacent position. The two steps of the Sonogashira–Hagihara coupling reactions from 1,4-dibromo-2,5-diiodobenzene (**1**) to 1,4-bis(2′-phenylethyn-1′-yl)-2,5-bis(2′-trimethylsilylethyn-1″-yl)benzene (**3a**) followed by the deprotection of K_2CO_3 afforded 1,4-diethynyl-2,5-bis(2′-phenylethyn-1′-yl)-benzene (**3a′**). Then, treatment with decaborane ($B_{10}H_{14}$) in the presence of *N*,*N*-dimethylaniline and the successive regioselective alkyne-insertion reaction afforded **CBH**. Similarly, **CBMe** was also synthesized by the two steps of the Pd-catalyzed coupling reactions followed by the alkyne-insertion reaction with decaborane, although the reaction yield was low due to steric hindrance. **CBH** and **CBMe** were stable to H_2O, air, and heat in both the solution and solid states at least for half a year. The structures of the obtained compounds were characterized by ^{1}H, ^{11}B and ^{13}C NMR spectroscopies and high-resolution mass analyses (Charts S1–S6, ESI†).

The structure of **CBH** was successfully confirmed by the X-ray crystallographic analysis (Fig. 1, Table S1, ESI†). The dihedral angle C2–C1–C3–C4 (φ) of **CBH** was 21°. This fact indicates that the 1,4-bis(phenylethynyl)benzene moiety has approximately a co-planar structure including the C1–C2 bond. In the crystal packing diagrams, **CBH** showed π-stacks with a distance of 4.190 Å between the phenyl rings of 1,4-bis(phenylethynyl)benzene moieties. It was presumed that steric repulsion of bulky icosahedral carborane clusters could be responsible for these structures.

The electronic properties of **CBH** in the ground state were examined by UV-vis absorption measurements. Fig. 2a shows the UV-vis absorption spectra of **CBH** and the model compound **M** (1,4-bis(phenylethynyl)benzene) in THF solution (1.0×10^{-5} M). **CBH** exhibited a large absorption band in the UV region ($\varepsilon > 35\,000$ M^{-1} cm^{-1}) assigned to the π–π* transition in the 1,4-bis(phenylethynyl)benzene moiety that corresponded to that of **M**. As listed in Table 1, the absorption band of **CBH** (λ_{max} = 344 nm) was obtained in a longer wavelength region compared to that of **M** (λ_{max} = 320 nm). It was proposed that the effect of the strong electron-accepting character of *o*-carborane can contribute to constructing a significant electronic interaction

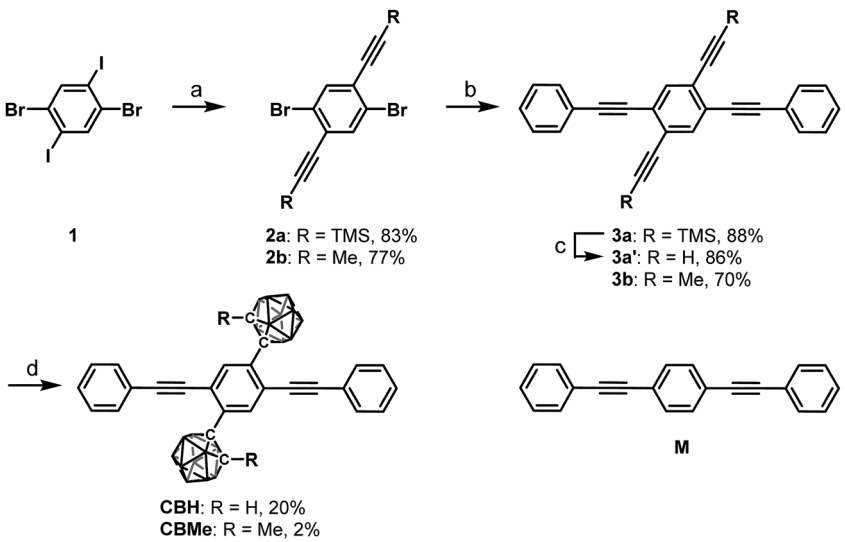

Scheme 1 Synthesis of **CBH** and **CBMe**. [a] *Reagents and conditions*: (a) ethynyl compound, $Pd(PPh_3)_4$, CuI, THF, $^iPr_2NH$, r.t., 36 h; (b) phenylacetylene, $Pd(PPh_3)_4$, CuI, THF, Et_3N, reflux, 22 h for **3a**, 48 h for **3b**; (c) K_2CO_3, THF, MeOH, r.t., 4 h; (d) decaborane, *N*,*N*-dimethylaniline, toluene, reflux, 7 d for **CBH**, 5 d for **CBMe**.

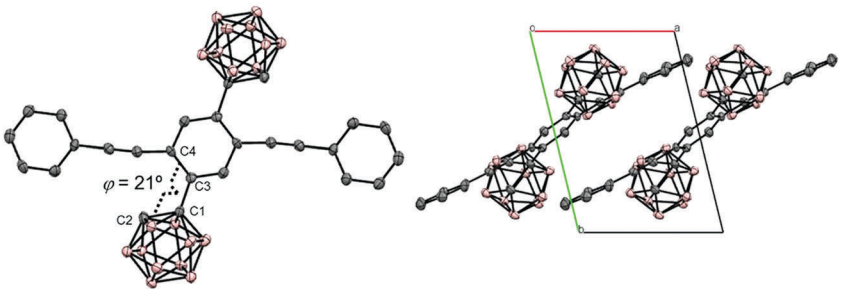

Fig. 1 Molecular structure and packing diagrams of **CBH** (hydrogen atoms are omitted for clarity, and thermal ellipsoids are displayed at 30% probability).

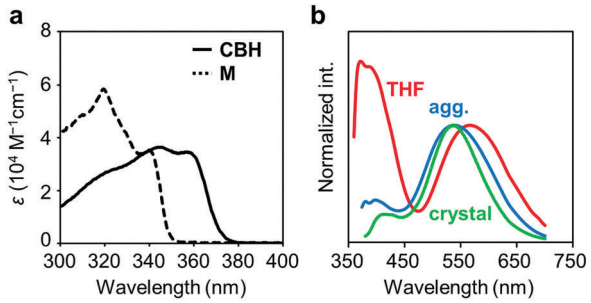

Fig. 2 (a) UV-vis absorption spectra of **CBH** and **M** (1.0×10^{-5} M) and (b) normalized PL spectra of **CBH** in THF solution (1.0×10^{-5} M), aggregates (THF/H_2O v/v = 1/99 solution, 1.0×10^{-5} M) and the crystal.

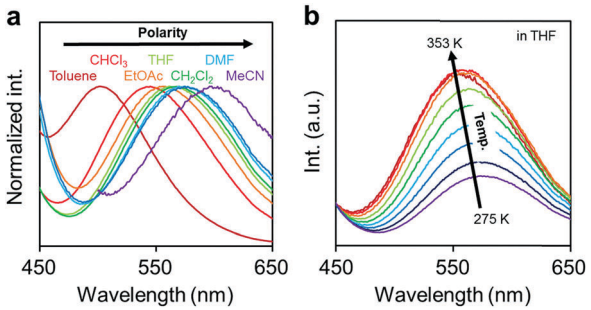

Fig. 3 (a) Solvent and (b) temperature-dependent peak shifts in the PL spectra of the solutions containing **CBH** (1.0×10^{-6} M).

Table 1 Summary of optical properties of the compounds

	THF[a]					Aggregation[b]		Crystal	
	λ_{abs} [nm]	ε [M^{-1} cm^{-1}]	E_g[c] [eV]	λ_{em} [nm]	Φ_{PL}[d]	λ_{em} [nm]	Φ_{PL}[d]	λ_{em} [nm]	Φ_{PL}[d]
CBH	344	36 300	3.33	371, 566	0.30	538	0.36	537	0.57
CBMe	368	39 200	3.23	540	0.84	542	0.81	493	0.78
M	320	58 500	3.55	347	0.95<	—[e]	—[e]	—[e]	—[e]

[a] Measured in THF solution (1.0×10^{-5} M). [b] Measured in THF/H_2O v/v = 1/99 solution (1.0×10^{-5} M). [c] Calculated from the onset value in the absorption spectra. [d] Determined as an absolute value with the integration sphere method. [e] Not detectable.

between the conjugated moiety and the *o*-carborane unit, followed by the peak shift *via* extension of π-conjugation to the whole molecule.

Next, the emission properties of **CBH** were investigated. The most impressive point was the dual-emissive property of **CBH** in the solution (Fig. 2b). Sharp emission bands with vibrational structures and broad ones were observed with peaks at around 370 nm and 570 nm, respectively. According to the previous reports, it was presumed that the aryl-modified *o*-carboranes can present ICT emission.[52] To elucidate the emission mechanism of **CBH**, optical spectra in various solvents (toluene, $CHCl_3$, EtOAc, THF, CH_2Cl_2, DMF and MeCN) were measured, and the Lippert–Mataga plots were prepared (Fig. 3a and Fig. S1, Table S2, ESI†). By increasing solvent polarity, solvatochromism was detected only from the bands around 570 nm. These data including the degree of Stokes shifts calculated with the position of the absorption bands clearly indicate that the emission bands around 370 nm and 570 nm are from the LE and ICT states, respectively. Lower emission efficiencies were obtained from the modified carboranes than from **M**. It is known that molecular motions including rotation at the connecting bond to the aryl moiety and vibration at the C–C bond in the *o*-carborane unit in the solution state should induce excitation deactivation along non-radiation processes.[30] Thus, emission annihilation was observed.

To evaluate the TICT character, the influence of molecular rotation on luminescence properties was examined by changing temperature. Thermochromic luminescence properties were observed. From the spectra in Fig. 3b, it was shown that the intensity of the emission band from the ICT state was enhanced by heating. This is reasonable because the transition from LE to ICT should be assisted by heating. Furthermore, it should be noted that only the LE emission was detected in the frozen state at 77 K where the molecular structure should be fixed at the initial state (Fig. S2, ESI†). This result means that structural alteration from the planar conformation, which can provide the LE emission, should proceed in the excited state followed by the exhibition of the ICT emission. From these data, the luminescence mechanism of **CBH** can be summarized. In the ground state, the planar conformation is dominant, leading to the LE emission. On exposure to photo-excitation, molecular rotation occurs, resulting in the formation of the ICT state. Finally, the emission band with environmental responsivity in the longer wavelength region was observed. Due to steric hindrance of the 1,4-bis(phenylethynyl)benzene moiety, rotation

was disturbed to some extent. Thus, the dual emissive property was obtained.

The solid-state emission properties of **CBH** were evaluated (Fig. 2b and Table 1). Interestingly, larger emission efficiencies were observed in both the aggregation state prepared by adding water to the THF solution and in the crystalline state. These data confirm that **CBH** has AIEE and CIEE properties. Similarly to the previous reports on aryl-modified *o*-carboranes, the *o*-carborane units should inhibit intermolecular motions in the condensed state because of steric hindrances. Thereby, ACQ was suppressed. In the previous report, it was shown that the formation of the TICT state was allowed even in the crystalline state. To evaluate the possibility of solid-state TICT formation with **CBH**, a photoluminescence (PL) spectrum was monitored at 77 K (Fig. S3, ESI†). Obviously, the emission band from the ICT state disappeared and only the LE emission was obtained. The same discussion based on the TICT mechanism should be applicable to that in the solution.

Next, by introducing the methyl groups at the adjacent carbon in the *o*-carborane units, the influence on optical properties was investigated. Synthesis was performed according to Scheme 1, and the characterization data indicated that the product has the desired structure. Unfortunately, a suitable single-crystal sample for X-ray crystallography was not obtained. However, it was suggested that the molecular structure should be fixed to the twisted conformation, which is similar to the structure in the TICT state.

Several comparison studies were carried out for evaluating the influence of the substituent effect on electronic properties. Fig. 4a shows the UV-vis absorption spectra of **CBMe** in THF solution (1.0×10^{-5} M). The sharp peak around 260 nm and the broad peak around 370 nm assigned to the π–π* transition band of the 1,4-bis(phenylethynyl)benzene moieties were observed. The values of the optical band gaps (E_g), which were estimated from the onset wavelength of the UV-vis absorption spectra, were in the order of **CBH** > **CBMe** (Table 1). The LUMO energy level was estimated from cyclic voltammetry (Fig. S4, ESI†) peak onset potentials, and the HOMO energy level was calculated from the LUMO energy level and the band gap energy estimated from the absorption edge (Table S3, ESI†). **CBH** and **CBMe** showed low-lying LUMO energy levels, −3.06 eV and −3.18 eV, respectively. By introducing the adjacent methyl groups into the *o*-carborane units, the molecular structure is anchored at the twisted conformation. According to the previous work, the electron-accepting ability of *o*-carborane is maximized at the twisted conformation.[52] Thus, a low-lying LUMO was realized, as observed in the cyclic voltammograms, leading to the narrower band-gap energy of **CBMe** than that of **CBH**.

The emission properties of **CBMe** were evaluated in various states (Fig. 4b). From the THF solution, a single emission band was observed with a peak at around 550 nm. From the PL spectra in various solvents followed by the analysis with the Lippert–Mataga plots, it was indicated that this broad emission band should result from the ICT state (Fig. S5, ESI†). Interestingly, **CBMe** showed high quantum efficiencies in the aggregate

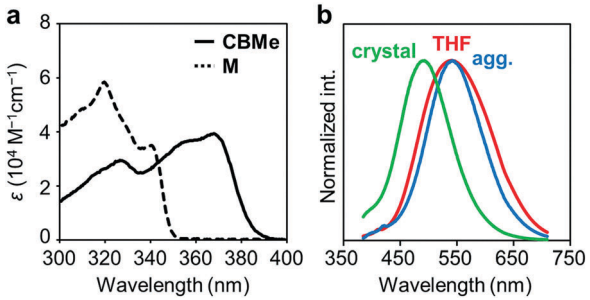

Fig. 4 (a) UV-vis absorption spectra of **CBMe** and **M** (1.0×10^{-5} M) and (b) normalized PL spectra of **CBMe** in THF solution (1.0×10^{-5} M), aggregates (THF/H_2O v/v = 1/99 solution, 1.0×10^{-5} M) and the crystal.

state (Φ_{PL} = 0.81), the crystalline state (Φ_{PL} = 0.78) and even in solution (Φ_{PL} = 0.84). It is assumed that excitation deactivation induced by the intramolecular motion at the *o*-carborane unit could be restricted by the substituent effect.[55] Furthermore, the molecular structure was fixed at the twisted conformation. As a consequence, ICT should be efficiently induced in the excited state. This speculation can be supported by the result from the solid-state emission at 77 K (Fig. S6, ESI†). Significant changes were hardly obtained by cooling the crystalline sample of **CBMe**. Molecular motions should be effectively suppressed by the methyl substituent.

Another notable point was the difference in emission wavelengths between the amorphous and crystalline samples (Fig. 4b and Table 1). It should be mentioned that the crystalline sample of **CBMe** provided the emission band in a shorter wavelength region than those in the amorphous state as well as in solution. In other words, **CBMe** was expected to present environment-sensitive luminescence properties. By taking into consideration this assumption, the mechanochromic luminescence properties were examined with **CBMe**. The crystalline sample was pounded in a mortar until the detectable peaks were eliminated in the X-ray diffraction analysis (Fig. S7, ESI†). During the mechanical treatments, the optical spectra were monitored (Fig. 5). Initially, the emission band was observed at 493 nm (Φ_{PL} = 0.78). It was shown that the peak position was shifted to a longer wavelength region by the treatment (λ_{em} = 516 nm, Φ_{PL} = 0.61). These data clearly indicate that **CBMe** has mechanochromic luminescence properties. Compared with the aggregation experiment with **CBMe**, as shown in Fig. 4, the emission band shift proceeded to the reverse direction by the formation of an amorphous state. In the solution-based system, solvent polarity should be responsible for emission properties. Therefore, the blue-shift might be induced by being surrounded by hydrophobic molecules. In the solid state, the degree of molecular packing should play a critical role in the electronic states. Because of bulky units including *o*-carboranes and methyl groups in **CBMe**, intermolecular interactions might be disturbed in the crystal packing, and blue-shifted emission was obtained. By the mechanical treatment, the molecular distribution should be randomized, and subsequently stabilization of energy levels by π-stacking followed by red-shifted emission could be realized. This scenario was also

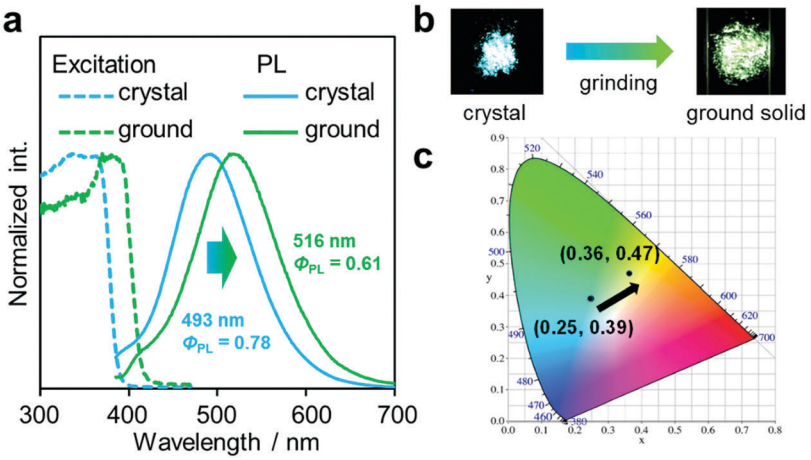

Fig. 5 (a) PL and excitation spectra of the solid samples of **CBMe**. (b) Pictures of the solid samples under UV irradiation before and after grinding. (c) Luminescent colors of the samples on the CIE diagram.

supported by the blue-shifted excitation spectrum. In the ground state, non-specific interactions could be formed. In the commodity mechanochromic luminescent materials, critical reduction of emission efficiencies was often induced after grinding, whereas **CBMe** presented a slight reduction of emission efficiency. The spherical molecular shape of *o*-carborane should be responsible for exhibiting environment-resistant intense emission by suppressing ACQ.

To deeply understand the TICT behavior of **CBH**, quantum chemical calculations were performed at the B3LYP/6-31+G(d)//B3LYP/6-31+G(d) level. Two geometries having planar (φ = 180°) and twisted (φ = 96°) conformers were obtained from the estimation for the optimized S_1 structure of **CBH**. The molecular orbitals involved in the electronic transition are shown in Fig. 6. It was found that the S_1–S_0 electronic transition in both conformers should be mainly derived from the lowest unoccupied molecular orbital (LUMO) to the highest occupied molecular orbital (HOMO); 95% for the planar and 98% for the twisted conformers. HOMOs in both conformers and the LUMO in the planar conformer were mainly on the 1,4-bis(phenylethynyl)benzene moiety, while the LUMO in the twisted conformer was significantly delocalized to the *o*-carborane unit. These results strongly support that the emission from the LE and ICT states was derived from the planar and twisted conformers, respectively. The calculated emission wavelengths for the LE and TICT states were 400 nm and 733 nm, respectively. In addition, the C–C bond length in the *o*-carborane unit was 1.66 Å in the planar conformer and 2.40 Å in the twisted conformer, indicating that stronger electron-withdrawing should occur in the twisted conformer.[52] This fact corresponded to the ICT character of the emission band from the twisted conformer. Finally, we evaluated the possibility of solid-state TICT in the crystalline state. From the calculation with the structure determined by X-ray crystallography (φ = 21°), it was shown that the HOMO and LUMO were localized mainly at the 1,4-bis(phenylethynyl)benzene moiety. Moreover, according to the experimental result, the calculated emission wavelength was 395 nm. From these data, it was

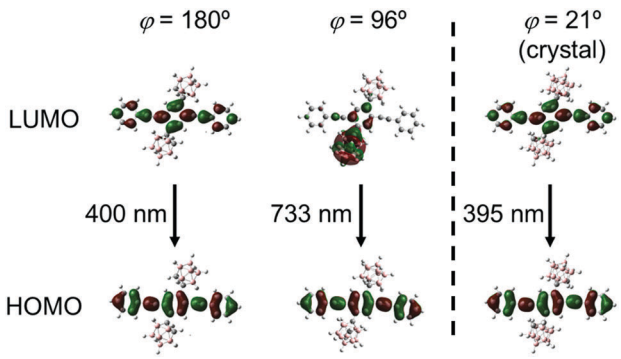

Fig. 6 Frontier orbitals involved in the S_1–S_0 transition for **CBH** at different 1,4-bis(phenylethynyl)benzene orientations (φ = 180°, 96° and 21°).

proposed that **CBH** can exhibit only emission from the LE state. Indeed, the corresponding emission band was obtained at 77 K; meanwhile, the emission from the ICT state was mainly observed in the far longer wavelength region (Fig. S3, ESI†). These data strongly suggest that **CBH** should form the TICT excited state even in the crystalline state.

The S_0–S_1 electronic transition was investigated by using the same level of calculation (Fig. 7). Compared with the model compound **M**, the energy levels of both the HOMO and LUMO of **CBH** were lower by 0.56 eV and 0.76 eV, respectively. The large decreases in energy levels of the frontier orbitals could be presumably derived from the strong electron-withdrawing character of the *o*-carborane unit, resulting in a lower band gap than **M**. These results showed good agreement with the red-shift of the absorption maximum and electrochemical data of **CBH** (Fig. 2 and Fig. S4, ESI†).

To support the optical properties of **CBMe**, DFT and TD-DFT calculations were carried out at the B3LYP/6-31+G(d)//B3LYP/6-31+G(d) level (Fig. S8 and S9, ESI†). From the structural optimization, an almost perpendicular conformation to the C–C bond in *o*-carborane (φ = 97°) was obtained and the transition wavelength was almost the same as that in the absorption spectrum. As shown in the results from the TD-DFT calculation, the

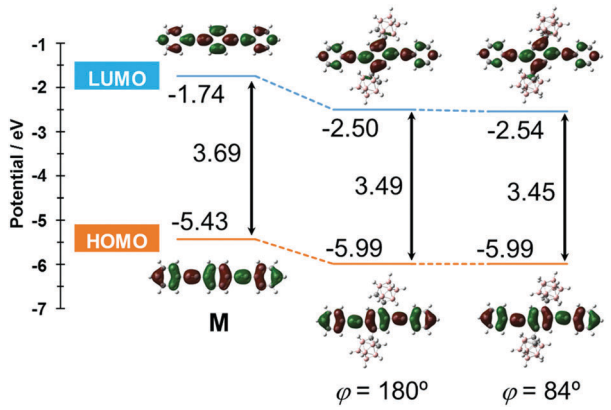

Fig. 7 Frontier orbitals involved in the S_0–S_1 transition and their energy levels for **CBH** and **M** at the B3LYP/6-31+G(d) level of theory.

frontier orbitals involved in the S_1–S_0 transition were mainly derived from the LUMO to HOMO transition (98%). The HOMO was found mostly on the 1,4-bis(phenylethynyl)benzene unit, while the LUMO was localized on the *o*-carborane unit with substantial orbital contribution, which is similar to the case of **CBH** (Fig. 6). These results strongly suggest that the emission around 490 nm originates from the ICT excited state. In addition, the LUMO partly existed on the C–H bond in the methyl group. This fact implies that the electron donation of the C–H antibonding orbital (σ*) of the methyl group into the σ* orbital on C–C in *o*-carborane could decrease the electron-withdrawing ability of the *o*-carborane unit.[52] This effect could induce a slightly higher LUMO level followed by a larger band gap, and it is implied that the observation of the emission band in the shorter wavelength region compared to that of **CBH** could be induced (Table S4, ESI†). The calculations for emission wavelengths of the ICT emission (733 nm for **CBH** and 692 nm for **CBMe**) also supported this issue. Due to the presence of the methyl group on the adjacent carbon in the *o*-carborane unit, the molecular conformation is restricted. As a result, limitation to the ICT character can be induced, followed by relatively-blue-shifted emission compared to that of the H-substituted compound, according to the previous report on emission properties of the series of anthracene–*o*-carborane dyads with various substituents.[55] A similar tendency in the emission wavelength was also suggested in this study.

Conclusion

It was demonstrated that the methyl substituent in the *o*-carborane unit dramatically influenced optical properties including luminescent color, emission intensity and sensitivity to external stimuli and environmental responsiveness in the bis-*o*-carborane-substituted 1,4-bis(phenylethynyl)benzene system. Basically, these changes can be explained by the degree of molecular motions and structures determined by the substituents. As a consequence, a variety of useful functions for developing advanced optical materials were obtained. Furthermore, according to computer calculation data, it was implied that dual *o*-carborane units might individually play different roles from each other in the electronic conjugation in the excited state. This speculation could be valid for establishing design strategies not only to precisely control emission efficiencies by external stimuli and environmental factors but also to increase the diversity of luminescence chromic behaviors.

Conflicts of interest

There are no conflicts to declare.

Acknowledgements

This work was partially supported by The Kyoto Technoscience Center (for K. T.) and a Grant-in-Aid for Scientific Research on Innovative Areas "New Polymeric Materials Based on Element-Blocks (No. 2401)" (JSPS KAKENHI Grant Number JP24102013).

References

1 Y. Chujo and K. Tanaka, *Bull. Chem. Soc. Jpn.*, 2015, **88**, 633–643.
2 M. Gon, K. Tanaka and Y. Chujo, *Polym. J.*, 2018, **50**, 109–126.
3 K. Tanaka and Y. Chujo, *NPG Asia Mater.*, 2015, **7**, e223.
4 H. Yamane, S. Ohtani, K. Tanaka and Y. Chujo, *Tetrahedron Lett.*, 2017, **58**, 2989–2992.
5 H. Yamane, K. Tanaka and Y. Chujo, *Tetrahedron Lett.*, 2015, **56**, 6786–6790.
6 K. Suenaga, K. Tanaka and Y. Chujo, *Chem. – Eur. J.*, 2017, **23**, 1409–1414.
7 M. Yamaguchi, S. Ito, A. Hirose, K. Tanaka and Y. Chujo, *J. Mater. Chem. C*, 2016, **3**, 5314–5319.
8 M. Yamaguchi, S. Ito, A. Hirose, K. Tanaka and Y. Chujo, *Mater. Chem. Front.*, 2017, **1**, 1573–1579.
9 K. Tanaka and Y. Chujo, *Macromol. Rapid Commun.*, 2012, **33**, 1235–1255.
10 R. Yoshii, A. Nagai, K. Tanaka and Y. Chujo, *Macromol. Rapid Commun.*, 2014, **35**, 1315–1319.
11 K. Tanaka, T. Yanagida, A. Hirose, H. Yamane, R. Yoshii and Y. Chujo, *RSC Adv.*, 2015, **5**, 96653–96659.
12 H. Yeo, K. Tanaka and Y. Chujo, *Macromolecules*, 2016, **49**, 8899–8904.
13 H. Yamane, S. Ito, K. Tanaka and Y. Chujo, *Polym. Chem.*, 2016, **7**, 2799–2807.
14 R. Yoshii, K. Tanaka and Y. Chujo, *Macromolecules*, 2014, **47**, 2268–2278.
15 S. Ito, A. Hirose, M. Yamaguchi, K. Tanaka and Y. Chujo, *Polymers*, 2017, **9**, 68–78.
16 A. Hirose, K. Tanaka, R. Yoshii and Y. Chujo, *Polym. Chem.*, 2015, **6**, 5590–5595.
17 K. Suenaga, R. Yoshii, K. Tanaka and Y. Chujo, *Macromol. Chem. Phys.*, 2016, **217**, 414–417.
18 R. Yoshii, K. Suenaga, K. Tanaka and Y. Chujo, *Chem. – Eur. J.*, 2015, **21**, 7231–7237.

19 K. Suenaga, K. Tanaka and Y. Chujo, *Eur. J. Org. Chem.*, 2017, 5191–5196.
20 S. Ohtani, M. Gon, K. Tanaka and Y. Chujo, *Chem. – Eur. J.*, 2017, **23**, 11827–11833.
21 T. Matsumoto, H. Takamine, K. Tanaka and Y. Chujo, *Mater. Chem. Front.*, 2017, **1**, 2368–2375.
22 K. Suenaga, K. Tanaka and Y. Chujo, *Chem. – Eur. J.*, 2017, **23**, 1409–1414.
23 S. Ito, A. Hirose, M. Yamaguchi, K. Tanaka and Y. Chujo, *J. Mater. Chem. C*, 2016, **3**, 5564–5571.
24 V. I. Bregadze, *Chem. Rev.*, 1992, **92**, 209–223.
25 M. Scholz and E. Hey-Hawkins, *Chem. Rev.*, 2011, **111**, 7035–7062.
26 F. Issa, M. Kassiou and L. M. Rendina, *Chem. Rev.*, 2011, **111**, 5701–5722.
27 R. Núñez, I. Romero, F. Teixidor and C. Viñas, *Chem. Soc. Rev.*, 2016, **45**, 5147–5173.
28 R. Núñez, M. Terrés, A. Ferrer-Ugalde, F. F. D. Biani and F. Teixidor, *Chem. Rev.*, 2016, **116**, 14307–14378.
29 R. N. Grimes, *Carboranes*, Academic Press, Amsterdam, 2nd edn, 2011, pp. 301–540.
30 K. Tanaka, K. Nishino, S. Ito, H. Yamane, K. Suenaga, K. Hashimoto and Y. Chujo, *Faraday Discuss.*, 2017, **196**, 31–42.
31 K. Nishino, K. Hashimoto, K. Tanaka, Y. Morisaki and Y. Chujo, *Tetrahedron Lett.*, 2016, **57**, 2025–2028.
32 K. Nishino, Y. Morisaki, K. Tanaka and Y. Chujo, *New J. Chem.*, 2017, **15**, 10550–10554.
33 X. Li, H. Yan and Q. Zhao, *Chem. – Eur. J.*, 2016, **22**, 1888–1898.
34 S. Mukherjee and P. Thilagar, *Chem. Commun.*, 2016, **52**, 1070–1093.
35 L. Böhling, A. Brockhinke, J. Kahlert, L. Weber, R. A. Harder, D. S. Yufit, J. A. K. Howard, J. A. H. MacBride and M. A. Fox, *Eur. J. Inorg. Chem.*, 2016, 403–412.
36 L. Weber, J. Kahlert, R. Brockhinke, L. Böhling, J. Halama, A. Brockhinke, H.-G. Stammler, B. Neumann, C. Nervi, R. A. Harder and M. A. Fox, *Dalton Trans.*, 2013, **42**, 10982–10996.
37 J. Kahlert, L. Böhling, A. Brockhinke, H.-G. Stammler, B. Neumann, L. M. Rendina, P. J. Low, L. Weber and M. A. Fox, *Dalton Trans.*, 2015, **44**, 9766–9781.
38 Y.-J. Cho, S.-Y. Kim, M. Cho, W.-S. Han, H.-J. Son, D. W. Cho and S. O. Kang, *Phys. Chem. Chem. Phys.*, 2016, **19**, 9702–9708.
39 S.-Y. Kim, Y.-J. Cho, G. F. Jin, W.-S. Han, H.-J. Son, D. W. Cho and S. O. Kang, *Phys. Chem. Chem. Phys.*, 2015, **17**, 15679–15682.
40 K.-R. Wee, Y.-J. Cho, S. Jeong, S. Kwon, J.-D. Lee, I.-H. Suh and S. O. Kang, *J. Am. Chem. Soc.*, 2012, **134**, 17982–17990.
41 B. H. Choi, J. H. Lee, H. Hwang, K. M. Lee and M. H. Park, *Organometallics*, 2016, **35**, 1771–1777.
42 R. Furue, T. Nishimoto, I. S. Park, J. Lee and T. Yasuda, *Angew. Chem., Int. Ed.*, 2016, **55**, 7171–7175.
43 M. Uebe, A. Ito, Y. Kameoka, T. Sato and K. Tanaka, *Chem. Phys. Lett.*, 2015, **633**, 190–194.
44 Y. Kameoka, M. Uebe, A. Ito, T. Sato and K. Tanaka, *Chem. Phys. Lett.*, 2014, **615**, 44–49.
45 M. Eo, M. H. Park, T. Kim, Y. Do and M. H. Lee, *Polymer*, 2013, **54**, 6321–6328.
46 T. Kim, H. Kim, K. M. Lee, Y. S. Lee and M. H. Lee, *Inorg. Chem.*, 2013, **52**, 160–168.
47 A. Ferrer-Ugalde, J. Cabrera-González, E. J. Juárez-Pérez, F. Teixidor, E. Pérez-Inestrosa, J. M. Montenegro, R. Sillanpää, M. Haukka and R. Núñez, *Dalton Trans.*, 2017, **46**, 2091–2104.
48 J. J. Peterson, A. R. Davis, M. Were, E. B. Coughlin and K. R. Carter, *ACS Appl. Mater. Interfaces*, 2011, **3**, 1796–1799.
49 D. Tu, P. Leong, Z. Li, R. Hu, C. Shi, K. Y. Zhang, H. Yan and Q. Zhao, *Chem. Commun.*, 2016, **52**, 12494–12497.
50 W. Zhang, Y. Luo, Y. Xu, L. Tian, M. Li, R. He and W. Shen, *Dalton Trans.*, 2015, **44**, 18130–18137.
51 L. Zhu, X. Tang, Q. Yu, W. Lv, H. Yan, Q. Zhao and W. Huang, *Chem. – Eur. J.*, 2015, **21**, 4721–4730.
52 H. Naito, K. Nishino, Y. Morisaki, K. Tanaka and Y. Chujo, *Angew. Chem., Int. Ed.*, 2017, **56**, 254–259.
53 R. Núñez, P. Farràs, F. Teixidor, C. Viñas, R. Sillanpää and R. Kivekäs, *Angew. Chem., Int. Ed.*, 2006, **45**, 1270–1272.
54 K. Nishino, H. Yamamoto, K. Tanaka and Y. Chujo, *Org. Lett.*, 2016, **18**, 4064–4067.
55 H. Naito, K. Nishino, Y. Morisaki, K. Tanaka and Y. Chujo, *Chem. – Asian J.*, 2017, **12**, 2134–2138.
56 H. Naito, K. Nishino, Y. Morisaki, K. Tanaka and Y. Chujo, *J. Mater. Chem. C*, 2017, **4**, 10047–10054.
57 J. Cabrera-González, S. Bhattacharyya, B. Milián-Medina, F. Teixidor, N. Farfán, R. Arcos-Ramos, V. Vargas-Reyes, J. Gierschner and R. Núñez, *Eur. J. Inorg. Chem.*, 2017, 4575–4580.
58 D. Tu, P. Leong, S. Guo, H. Yan, C. Lu and Q. Zhao, *Angew. Chem., Int. Ed.*, 2017, **56**, 11370–11374.
59 L. Weber, J. Kahlert, R. Brockhinke, L. Böhling, A. Brockhinke, H.-G. Stammler, B. Neumann, R. A. Harder and M. A. Fox, *Chem. – Eur. J.*, 2012, **18**, 8347–8357.
60 H. Naito, Y. Morisaki and Y. Chujo, *Angew. Chem., Int. Ed.*, 2015, **54**, 5084–5087.
61 K. Nishino, H. Yamamoto, K. Tanaka and Y. Chujo, *Asian J. Org. Chem.*, 2017, **6**, 1818–1822.